Journal of Computational Mathematics, Vol.27, No.2-3, 2009, 280–298.

A NUMERICAL STUDY OF UNIFORM SUPERCONVERGENCE OF LDG METHOD FOR SOLVING SINGULARLY PERTURBED PROBLEMS*

Ziqing Xie, Zuozheng Zhang and Zhimin Zhang
Key Laboratory of Computational and Stochastic Mathematics and Its Applications, Universities of Hunan Province, Hunan Normal University, Changsha 410081, China
Email: ziqingxie@hunnu.edu.cn, zuozhengzhang@yahoo.cn, zzhang@math.wayne.edu

Abstract

In this paper, we consider the local discontinuous Galerkin method (LDG) for solving singularly perturbed convection-diffusion problems in one- and two-dimensional settings. The existence and uniqueness of the LDG solutions are verified. Numerical experiments demonstrate that it seems impossible to obtain uniform superconvergence for numerical fluxes under uniform meshes. Thanks to the implementation of two-type different anisotropic meshes, i.e., the Shishkin and an improved grade meshes, the uniform $2p+1$-order superconvergence is observed numerically for both one-dimensional and two-dimensional cases.

Mathematics subject classification: 65N30.
Key words: Singularly perturbed problems, Local discontinuous Galerkin method, Numerical fluxes, Uniform superconvergence.

1. Introduction

The discontinuous Galerkin method (DGM) was first introduced in 1973 by Reed and Hill [25] for solving the neutron transport equation. Successively in 1974, Lesaint and Raviart [20] made the first analysis for the linear advection equation. Since then there has been an active development of DGM for hyperbolic, elliptic, and parabolic partial differential equations. For a fairly thorough compilation of the history of these methods and their applications see [15].

The local discontinuous Galerkin (LDG) method was first proposed by Cockburn and Shu in [11] as a generalization of the DGM proposed by Bassi and Rebay [2] for the compressible Navier-Stokes equations. In [11] the stability and error estimates for the method were studied. The first convergence analysis of the LDG method for elliptic problems was given by P. Castillo *et al.* [9]. Actually the LDG method possesses several properties which make it popular for practical computations. The LDG method is local (element-wise) conservative, a property which is particularly difficult to preserve by high-order finite elements. This method is also suitable for hp-adaptive implementation and allows a very efficient parallelization. A more detail review about the LDG method was given in [7, 15].

In recent years the numerical solutions of singularly perturbed boundary value problems have been received much attention. There are numerous papers, see, e.g., [6, 21, 23, 24, 30, 34–36], written on this subject. A book by Roos *et al.* [27] provides an extensive list of literature on this topic. One of the difficulties in numerically computing the solution of singularly perturbed problems lays in the so-called boundary layer behavior, i.e., the solution varies very rapidly in a very thin layer near the boundary.

* Received December 31, 2007 / Revised version received May 10, 2008 / Accepted June 22, 2008 /

Currently, there are mainly two ways to solve this problem. The first way is through the use of the h version on layer-adapted meshes [6, 26, 35, 36]. The uniform convergence independent of the perturbation parameter ε can be obtained when this technique is used. The second alternative is through the use of p or hp version [29, 32, 33]. The exponent rates of convergence can be established when the domain is smooth.

In [10], Celiker and Cockburn investigated the superconvergence of the numerical traces of some DG methods at the nodes of the mesh for 1-D convection-diffusion problems. Particularly, the authors proved that the superconvergence order of both numerical traces $\hat{u}_h^{\varepsilon}$ and $-\hat{q}_h + c\hat{u}_h^{c}$ is $2p+1$ when polynomials of degree at most p are used for the approximation (q_h, u_h) based on a suitably designed LDG method. Nevertheless in that paper, the uniform superconvergence of numerical traces was not investigated as the diffusion parameter ε goes to zero.

In [7], Castillo *et al.* showed, for special numerical fluxes, that the LDG method converges with the optimal rate of convergence of order h^{p+1} in the energy norm for the model problem of constant-coefficient linear convection-diffusion equation in the one spacial dimension. The first a priori error analysis of the LDG method for purely elliptic problems was given by Castillo *et al.* [9]. In this paper, meshes including elements of various shapes and general numerical fluxes were studied. It was shown that the convergence rates of the error in u and ∇u in the L^2 norm are $k+\frac{1}{2}$ and k, respectively. In [16], Cockburn *et al.*, established the superconvergence of the LDG method for multidimensional elliptic problems on Cartesion grids with special numerical fluxes. The convergence order in L^2 norm of the error in u and ∇u are $k+1$ and $k+\frac{1}{2}$, respectively, when tensor product polynomials of degree at most k are used. Comparing with the results in [9], the error bounds was improved by a factor $\sqrt{h}$. In this sense, it is a superconvergence result. Actually it is an extension to the multidimensional case of the results obtained by Castillo *et al.* [7, 8].

In [34], Xie and Zhang studied the LDG method for solving singularly perturbed convection-diffusion problems with mixed boundary condition. Their numerical test results indicate that the LDG method does not produce any oscillation outside the boundary layer region even under uniform mesh for small ε. The superconvergence rate $\mathcal{O}(h^{2p+1})$ of the numerical traces at the nodes was also proved.

In this paper we will compare two-type layer-adapted meshes when they are used in the h version of the LDG method for one and two dimensional problems. The numerical results exhibit that the LDG method does not produce any oscillation even under uniform meshes for arbitrary ε for both 1-D and 2-D cases. On the other hand, the $2p+1$ order uniform superconvergence of numerical fluxes are observed numerically for the LDG method under both the Shishkin and an improved grade meshes. Here the so-called "uniform convergence" means that the convergence rate is uniformly valid with respect to ε. It is worthwhile to point out that theoretical analysis of the uniform convergence is extremely difficult and remains an open problem for the LDG method.

The rest of this paper is organized as follows: In Section 2, the construction of the Shishkin mesh and improved grade mesh is described. The LDG method for one and two dimensions will be introduced in Section 3. In Section 4, the analysis of existence and uniqueness of the LDG solution is exhibited. We will in Section 5 present fruitful numerical results which illustrate the robustness of the LDG method for solving singularly perturbed problems based on two type layer-adapted meshes mentioned above. We end this paper with some conclusions in the final section.

2. Shishkin Mesh and Improved Grade Mesh

2.1. Shishkin mesh

The Shishkin meshes proposed by Shishkin are piecewise uniform meshes that are adapted to the layer structure of the singularly perturbed problems. First, we consider Shishkin mesh in one-dimensional interval $[0,1]$. For the implementation in our model problem in Section 3, which has a boundary layer at the outflow boundary $x=1$, the construction of Shishkin mesh is to choose a prior mesh transition parameter τ which denotes the approximate width of the boundary layer. Then the intervals $(0,1-\tau)$ and $(1-\tau,1)$ are each divided into $N/2$ equal subintervals with N even. The set of mesh points for the one dimension can be denoted by

$$\Omega^N = \{x_i : i = 1, \cdots, N+1\},$$

where

$$x_i = \begin{cases} 2(i-1)(1-\tau)/N, & i = 1, \cdots, 0.5N+1, \\ 1-2(N+1-i)\tau/N, & i = 0.5N+2, \cdots, N+1. \end{cases} \tag{2.1}$$

So the length of element is given by

$$h_j = \begin{cases} 2(1-\tau)/N, & j = 1, \cdots, 0.5N, \\ 2\tau/N, & j = 0.5N+1, \cdots, N. \end{cases} \tag{2.2}$$

Thus the global mesh is piecewisely uniform.

The Shishkin mesh for 2-D is constructed for both x and y directions in a tensor product way. Still let τ_x and τ_y denote two mesh transition parameters which reflect the approximate width of the boundary layer. In our model problems, we take $\tau = \tau_x = \tau_y$ for simplicity. So the domain Ω is divided into four subdomains

$$\Omega_0 = (0,1-\tau)^2, \qquad \Omega_x = (1-\tau,1)\times(0,1-\tau),$$
$$\Omega_y = (0,1-\tau)\times(1-\tau,1), \qquad \Omega_{xy} = (1-\tau,1)^2.$$

An example of the Shishkin mesh for 2-D is shown in Fig 2.1 with $\tau = 0.1$ and $N = 16$. We specify a set of mesh points for the two dimension, i.e.,

$$\Omega^N = \{(x_i, y_j) \in \Omega : i, j = 1, \cdots, N+1\}$$

by

$$x_i = \begin{cases} 2(i-1)(1-\tau)/N, & i = 1, \cdots, 0.5N+1, \\ 1-2(N+1-i)\tau/N, & i = 0.5N+2, \cdots, N+1, \end{cases} \tag{2.3}$$

$$y_j = \begin{cases} 2(j-1)(1-\tau)/N, & j = 1, \cdots, 0.5N+1, \\ 1-2(N+1-j)\tau/N, & j = 0.5N+2, \cdots, N+1. \end{cases} \tag{2.4}$$

2.2. Improved grade mesh

The Shishkin mesh introduced in the above subsection can be modified to obtain another layer-adapted mesh which is denoted by improved grade mesh. It may be obtained by properly selecting the mesh generating function in [22]. The detailed construction of improved grade meshes is defined below.

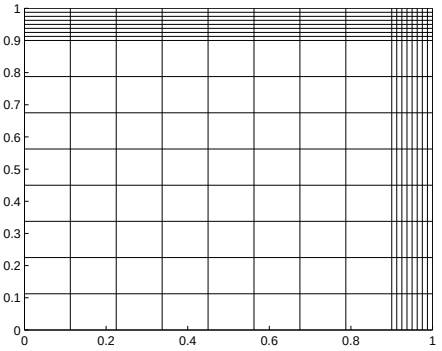

Fig. 2.1. Shishkin mesh.

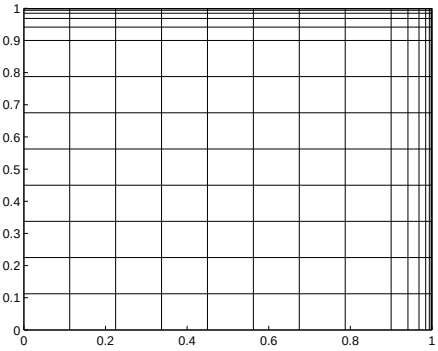

Fig. 2.2. Improved grade mesh.

First, we consider the 1-D case, choose a mesh transition parameter τ, which is the same as that in the definition of Shishkin mesh. The interval $\Omega = (0,1)$ is also divided into two parts $\Omega_1 = (0, 1-\tau)$ and $\Omega_2 = (1-\tau, 1)$. The first part Ω_1 is still divided into $N/2$ equal subintervals. Nevertheless, the interval Ω_2 is divided into $N/2$ non-uniform subintervals. Given a parameter $h = 2/N$, the partition $\{x_j\}_{j=1}^{N+1}$ of the interval $(0,1)$ are given by

$$x_j = \begin{cases} 0, & j = 1, \\ x_{j-1} + 2(1-\tau)/N, & j = 2, \cdots, 0.5N+1, \\ 1 - \tau((N+1-j)h)^\lambda, & j = 0.5N+2, \cdots, N+1. \end{cases} \tag{2.5}$$

where λ is a mesh parameter which is greater than or equal to 1 in practical computation. So the length of element is given by

$$h_j = \begin{cases} 2(1-\tau)/N & j = 1, \cdots, 0.5N, \\ x_{j+1} - x_j = \tau\big((N-j)h\big)^\lambda\big[(1+1/(N-j))^\lambda - 1\big] & j = 0.5N+1, \cdots, N-1, \\ x_{N+1} - x_N = \tau h^\lambda & j = N. \end{cases} \tag{2.6}$$

It is apparent that the Shishkin mesh is the special case of improved grade mesh with $\lambda = 1$. With increasing λ, more and more mesh points will concentrate in the neighborhood of 1. Consequently the solution is approximated well on the boundary layers.

Similar to the Shishkin mesh, the design of the improved grade mesh for the one dimensional case can be extended to the two dimensional case easily. We also specify a set of mesh points of improved grade meshes for the two dimensional case, i.e., $\Omega^N = \{(x_i, y_j) \in \Omega : i, j = 1, \cdots, N+1\}$, where

$$x_i = \begin{cases} 0, & i = 1, \\ x_{i-1} + 2(1-\tau)/N, & i = 2, \cdots, 0.5N+1, \\ 1 - \tau((N+1-i)h)^\lambda, & i = 0.5N+2, \cdots, N+1, \end{cases} \tag{2.7}$$

and

$$y_j = \begin{cases} 0, & j = 1, \\ y_{j-1} + 2(1-\tau)/N, & j = 2, \cdots, 0.5N+1, \\ 1 - \tau((N+1-j)h)^\lambda, & j = 0.5N+2, \cdots, N+1. \end{cases} \tag{2.8}$$

An example of improved grade mesh for 2-D is shown in Fig 2.2 with $\tau = 0.1$, $N = 16$ and $\lambda = 4$.

3. The Local Discontinuous Galerkin Method

3.1. One-dimensional problem

For the sake of simplicity, we consider the singularly perturbed convection-diffusion problem with Dirichlet boundary condition, i.e,

$$-\varepsilon u'' + bu' = f, \quad \text{in } \Omega = (0,1), \tag{3.1a}$$

$$u(0) = u_0, \quad u(1) = u_1, \tag{3.1b}$$

where $b > 0$ and ε is a small positive parameter. The choice of $b > 0$ guarantees that the location of the boundary layer is at the outflow boundary $x = 1$.

By setting $q = u'$, Eq. (3.1) can be rewritten as

$$-\varepsilon q' + bu' = f, \quad \text{in } (0,1), \tag{3.2a}$$

$$q - u' = 0, \quad \text{in } (0,1), \tag{3.2b}$$

$$u(0) = u_0, \quad u(1) = u_1. \tag{3.2c}$$

Denote the mesh by $I_j = [x_{j-\frac{1}{2}}, x_{j+\frac{1}{2}}]$ for $j = 1, 2, \cdots, N$ with $x_{\frac{1}{2}} = 0$, $x_{N+\frac{1}{2}} = 1$. The center of the cell is $x_j = (x_{j-\frac{1}{2}} + x_{j+\frac{1}{2}})/2$ and $h_j = |I_j|$. Set

$$h = \max_{1\le j\le N} h_j, \qquad \Omega_h = \bigcup_{j=1,\cdots,N} I_j.$$

We denote by $u^+_{j+\frac{1}{2}}$ and $u^-_{j+\frac{1}{2}}$ the values of u at $x_{j+\frac{1}{2}}$, from the right cell and the left cell of $x_{j+\frac{1}{2}}$, respectively. Denote the jump at $x_{j+\frac{1}{2}}$ by $[u_{j+\frac{1}{2}}] = u^+_{j+\frac{1}{2}} - u^-_{j+\frac{1}{2}}$. We multiply the first two equations of (3.2) by test functions v and w, separately, and integrate by parts in each cell I_j to obtain

$$\varepsilon \int_{I_j} qv'dx - b\int_{I_j} uv'dx - (\varepsilon q - bu)^-_{j+\frac{1}{2}} v^-_{j+\frac{1}{2}} + (\varepsilon q - bu)^+_{j-\frac{1}{2}} v^+_{j-\frac{1}{2}} = \int_{I_j} fvdx, \tag{3.3a}$$

$$\int_{I_j} uw'dx + \int_{I_j} qwdx - u^-_{j+\frac{1}{2}} w^-_{j+\frac{1}{2}} + u^+_{j-\frac{1}{2}} w^+_{j-\frac{1}{2}} = 0. \tag{3.3b}$$

This is the weak formulation we shall use to define the DG methods. We can now define the piecewise polynomial space V_h as the space of polynomials of degree $p \ge 1$ in each cell I_j, i.e.,

$$V_h = \{v : v \in P_p(I_j), \quad j = 1, 2, \cdots, N\}.$$

Moreover, we define the space

$$H^k(\Omega_h) = \{v : v \in H^k(I_j), \quad j = 1, 2, \cdots, N\}$$

with $k \ge 0$. We will search for an approximate solution of (3.2) in terms of piecewise polynomial function $u_h, q_h \in V_h$ that satisfy (3.2) in a weak sense. Following Cockburn and Shu [11], we consider the following general formulation:

Find $u_h, q_h \in V_h$ such that

$$\varepsilon \int_{I_j} q_h v'dx - b\int_{I_j} u_h v'dx - (\varepsilon \hat{q}_h - b\tilde{u}_h)_{j+\frac{1}{2}} v^-_{j+\frac{1}{2}} + (\varepsilon \hat{q}_h - b\tilde{u}_h)_{j-\frac{1}{2}} v^+_{j-\frac{1}{2}} = \int_{I_j} fvdx, \tag{3.4a}$$

$$\int_{I_j} u_h w'dx + \int_{I_j} q_h wdx - \hat{u}_{h\,j+\frac{1}{2}} w^-_{j+\frac{1}{2}} + \hat{u}_{h_{j-\frac{1}{2}}} w^+_{j-\frac{1}{2}} = 0, \tag{3.4b}$$

for any v and $w \in V_h$. To complete the specification of a DG method, one must define the numerical traces $\hat{q}_h$, $\hat{u}_h$ and $\tilde{u}_h$ at the nodes. Through the specification of the numerical traces, the interaction of u_h and q_h in different intervals I_j and the boundary conditions are imposed. The impact of the choice of the numerical traces on the DG method for solving the linear elliptic equation was shown in [1]. First we define the convective flux as the classical upwind one, i.e.,

$$\tilde{u}_{h_{\frac{1}{2}}} = u_0, \quad \tilde{u}_{h_{j+\frac{1}{2}}} = (u_h)^-_{j+\frac{1}{2}}, \quad j = 1, \cdots, N. \tag{3.5}$$

The LDG numerical fluxes are designed by Cockburn and Shu, i.e.

$$\hat{u}_{h_{j+\frac{1}{2}}} = \begin{cases} u_0, & j = 0, \\ \{u_h\}_{j+\frac{1}{2}} - C_{12} \cdot [u_h]_{j+\frac{1}{2}}, & j = 1, \cdots, N-1, \\ u_1, & j = N, \end{cases} \tag{3.6}$$

$$\hat{q}_{h_{j+\frac{1}{2}}} = \begin{cases} (q_h)^+_{\frac{1}{2}} & j = 0, \\ \{q_h\}_{j+\frac{1}{2}} + C_{12} \cdot [q_h]_{j+\frac{1}{2}}, & j = 1, \cdots, N-1, \\ q_h{}^-_{N+\frac{1}{2}} - \alpha\big((u_h)^-_{N+\frac{1}{2}} - u_1\big), & j = N, \end{cases} \tag{3.7}$$

where $\alpha = \max\{1, p\}\varepsilon/h_N$ and $C_{12} = 1/2$.

3.2. Two-dimensional problem

Consider the following two-dimensional convection-diffusion problem

$$-\varepsilon\Delta u + \vec{\beta} \cdot \nabla u = f, \quad \text{in } \Omega = (0,1) \times (0,1), \tag{3.8a}$$

$$u = u_0, \quad \text{on } \partial\Omega, \tag{3.8b}$$

where $\vec{\beta} = (\beta_1, \beta_2) \geq (\alpha, \alpha) > (0,0)$ and β_1, β_2 are constants, ε is a small parameter. By setting $q = \nabla u$, Eq. (3.8) can be rewritten as

$$q = \nabla u, \quad \text{in } \Omega, \tag{3.9a}$$

$$-\varepsilon\nabla \cdot q + \vec{\beta} \cdot \nabla u = f, \quad \text{in } \Omega, \tag{3.9b}$$

$$u = u_0, \quad \text{on } \partial\Omega. \tag{3.9c}$$

Multiplying the first two equations of (3.9) by test functions $r \in L^2(\Omega)^2, v \in L^2(\Omega)$, respectively and integrating them by parts over the rectangle k of the Cartesian grid $\mathcal{T}_h$ with which we triangulate the domain Ω, we obtain

$$\int_k q \cdot r dx = -\int_k u\nabla \cdot r dx + \int_{\partial k} ur \cdot n_k ds, \tag{3.10a}$$

$$\varepsilon\int_k q \cdot \nabla v dx - \int_k u\vec{\beta} \cdot \nabla v dx - \varepsilon\int_{\partial k} vq \cdot n_k ds + \int_{\partial k} uv\vec{\beta} \cdot n_k ds = \int_k fv dx, \tag{3.10b}$$

where n_k is the unit outward normal to ∂k. Next we will define the approximate solution (q_h, u_h) of the exact solution (q, u) in the finite element spaces M_N and V_N, where

$$M_N := \{q \in L^2(\Omega)^2 : \ q|_k \in S(k)^2, \ \ \forall k \in \mathcal{T}_h\},$$
$$V_N := \{u \in L^2(\Omega) : \ u|_k \in S(k), \quad \forall k \in \mathcal{T}_h\},$$

with $S(k) := Q^p(k)$={polynomials of degree at most p in each variable on k }.

Now we will search for the approximate solutions of (3.9) in terms of piecewise polynomial functions $q_h \in M_N$, $u_h \in V_N$, that satisfy (3.9) in a weak sense. The aim is to find $q_h \in M_N, u_h \in V_N$ such that for any $r \in M_N, v \in V_N$,

$$\int_k q_h \cdot r dx = -\int_k u_h \nabla \cdot r dx + \int_{\partial k} \hat{u}_h r \cdot n_k ds, \tag{3.11}$$

$$\varepsilon \int_k q_h \cdot \nabla v dx - \int_k u_h \vec{\beta} \cdot \nabla v dx - \varepsilon \int_{\partial k} v \hat{q}_h \cdot n_k ds + \int_{\partial k} \tilde{u}_h v \vec{\beta} \cdot n_k ds = \int_k f v dx. \tag{3.12}$$

The function $\hat{q}_h$, $\hat{u}_h$ and $\tilde{u}_h$ are the numerical fluxes which approximate the fluxes of u and q on the boundary of the elements. To define these numerical fluxes, we need to introduce some notations. We denote by Γ the union of the boundaries of the elements $k \in \mathcal{T}_h$ and Γ_0 the set of all interior faces of the triangulation $\mathcal{T}_h$. Let $\partial\Omega = \Gamma^+ \cup \Gamma^-$ denote the boundary of Ω with $\Gamma^+ := \{e \subset \partial\Omega : v \cdot n > 0\}$, $\Gamma^- := \{e \subset \partial\Omega : v \cdot n < 0\}$, where $v = [v_1, v_2]^T$ is a constant vector with $v_i > 0$, $(i = 1, 2)$ and n is the unit outward normal to $\partial\Omega$. In this paper, we take $v = [1, 1]^T$. Let e be an internal edge shared by two adjacent elements of k_1 and k_2. For any point $x \in e$, let n^+ and n^- be the corresponding outward unit normals at x. We first introduce the average value operator $\{\cdot\}$ and the jump operator $[\cdot]$, i.e.,

$$\{u\} := (u^+ + u^-)/2, \qquad [u] := u^+ n^+ + u^- n^-,$$
$$\{q\} := (q^+ + q^-)/2, \qquad [q] := q^+ \cdot n^+ + q^- \cdot n^-.$$

Next we will define the numerical fluxes with the notations above. If e is an internal boundary of Ω, the numerical fluxes are defined by

$$\hat{q}_h = \{q_h\} - C_{12}[q_h] - C_{11}[u_h], \quad \hat{u}_h = \{u_h\} + C_{12}[u_h]. \tag{3.13}$$

If e is an external boundary of Ω, the numerical fluxes are

$$\hat{q}_h = q_h^+ - C_{11}(u_h - u_0)n^+, \quad \hat{u}_h = u_0. \tag{3.14}$$

In (3.13) and (3.14), $C_{11} \geq 0$, C_{12} is a vector function such that $C_{12} \cdot n = \text{sign}(v \cdot n)/2$. The numerical flux associated with the convection is the classical upwind flux, namely,

$$\tilde{u} = \begin{cases} u_0, & \text{on } \Gamma^-, \\ \{u_h\} + D_{11} \cdot [u_h], & \text{on } \Gamma_0, \\ u_h^+, & \text{on } \Gamma^+, \end{cases} \tag{3.15}$$

where D_{11} is a vector function satisfying $D_{11}(i) > 0$, $i = 1, 2$. Actually, in Section 5, we take $C_{11} = 1, D_{11} = \left[\frac{1}{2}, \frac{1}{2}\right]^T$.

4. Existence and Uniqueness of the LDG Solutions

4.1. One-dimensional case

Proposition 4.1. *The LDG method defined by* (3.4) *with the numerical traces* (3.5), (3.6) *and* (3.7) *produces a unique solution.*

Proof. See Theorem 3.2 [37]. □

Remark 4.1. Existence and uniqueness of the LDG method under some other flux selections has been established elsewhere, see, e.g., [10].

4.2. Two-dimensional case

Proposition 4.2. *Consider the LDG method defined by the weak formulation* (3.11) *and* (3.12) *with the numerical fluxes* (3.13), (3.14) *and* (3.15). *If* $C_{11} \geq 0$, $D_{11}(i)\beta(i) > 0, i = 1, 2$, *then the LDG method defines a unique approximate solution* $(q_h, u_h) \in M_N \times V_N$ *of* (3.2).

Proof. Due to the linearity of the model problems (3.11) and (3.12), it is enough to show that the only solution to (3.11) and (3.12) with $f = 0$ is $q_h = 0$ and $u_h = 0$.

Denoting $T(\Gamma) := \Pi_{k\in T_h} L^2(\partial k)$, a straightforward computation shows that for $q_k \in T(\Gamma)$ and $\phi_k \in [T(\Gamma)]^2$,

$$\sum_{k\in T_h} \int_{\partial k} q_k \phi_k \cdot n_k ds = \int_\Gamma \{\phi\} \cdot [q] ds + \int_{\Gamma_0} \{q\}[\phi] ds. \tag{4.1}$$

By use of (4.1), we sum (3.11) over all the elements and obtain

$$\int_\Omega q_h \cdot r dx = -\int_\Omega u_h \nabla \cdot r ds + \int_\Gamma \{r\} \cdot [\hat{u}_h] ds + \int_{\Gamma_0} [r]\{\hat{u}_h\} dx, \tag{4.2}$$

which can be written by integration by parts as

$$\int_\Omega q_h \cdot r dx = \int_\Omega \nabla u_h \cdot r dx + \int_\Gamma \{r\} \cdot [\hat{u}_h - u_h] ds + \int_{\Gamma_0} [r]\{\hat{u}_h - u_h\} ds. \tag{4.3}$$

By implementing (4.1) again, Eq. (3.12) can be written as

$$\begin{aligned} &\varepsilon \int_\Omega q_h \cdot \nabla v dx - \int_\Omega u_h \nabla \cdot (\beta v) dx - \varepsilon \int_\Gamma \{\hat{q}_h\} \cdot [v] ds - \varepsilon \int_{\Gamma_0} [\hat{q}_h]\{v\} ds \\ &\quad + \int_\Gamma \{\beta v\} \cdot [\tilde{u}_h] ds + \int_{\Gamma_0} [\beta v]\{\tilde{u}_h\} ds = \int_\Omega f v dx. \end{aligned} \tag{4.4}$$

In (4.3) and (4.4), taking $r = q_h$ and $v = u_h$ implies

$$\|q_h\|_2^2 = \int_\Omega q_h \cdot \nabla u_h dx + \int_\Gamma \{q_h\} \cdot [\hat{u}_h - u_h] ds + \int_{\Gamma_0} [q_h]\{\hat{u}_h - u_h\}, \tag{4.5}$$

and

$$\begin{aligned} \int_\Omega q_h \cdot \nabla u_h dx = \frac{1}{\varepsilon}\Big[&\int_\Omega u_h \nabla \cdot (\beta u_h) dx - \int_\Gamma \{\beta u_h\} \cdot [\tilde{u}_h] ds - \int_{\Gamma_0} [\beta u_h]\{\tilde{u}_h\} ds\Big] \\ &+ \int_\Gamma \{\hat{q}_h\} \cdot [u_h] ds + \int_{\Gamma_0} [\hat{q}_h]\{u_h\} ds + \frac{1}{\varepsilon} \int_\Omega f u_h dx. \end{aligned} \tag{4.6}$$

Substituting (4.6) into (4.5), we obtain

$$\begin{aligned} &\|q_h\|_2^2 + \frac{1}{\varepsilon}\Big[- \int_\Omega u_h \nabla \cdot (\beta u_h) dx + \int_\Gamma \{\beta u_h\} \cdot [\tilde{u}_h] ds + \int_{\Gamma_0} [\beta u_h]\{\tilde{u}_h\} ds\Big] - \int_\Gamma \{\hat{q}_h\} \cdot [u_h] ds \\ &\quad - \int_{\Gamma_0} [\hat{q}_h]\{u_h\} ds - \int_\Gamma \{q_h\} \cdot [\hat{u}_h - u_h] ds - \int_{\Gamma_0} [q_h]\{\hat{u}_h - u_h\} ds \\ &= \frac{1}{\varepsilon} \int_\Omega f u_h dx. \end{aligned} \tag{4.7}$$

Again integration by parts and the implementation of (4.1) in (4.7) yields

$$\begin{aligned}\|q_h\|_2^2 + \frac{1}{\varepsilon}\Big\{ \int_\Omega (\beta u_h)\cdot\nabla u_h dx + \int_\Gamma \{\beta u_h\}\cdot[\tilde{u_h} - u_h]ds + \int_{\Gamma_0}[\beta u_h]\{\tilde{u}_h - u_h\}ds]\Big\} \\ - \int_\Gamma \{\hat{q}_h\}\cdot[u_h]ds - \int_{\Gamma_0}[\hat{q}_h]\{u_h\}ds - \int_\Gamma \{q_h\}\cdot[\hat{u}_h - u_h]ds - \int_{\Gamma_0}[q_h]\{\hat{u}_h - u_h\}ds \\ = \frac{1}{\varepsilon}\int_\Omega f u_h dx. \end{aligned} \tag{4.8}$$

By setting

$$I_1 = \frac{1}{\varepsilon}\int_\Omega (\beta u_h)\cdot\nabla u_h dx, \tag{4.9a}$$

$$I_2 = \frac{1}{\varepsilon}\{\int_\Gamma \{\beta u_h\}\cdot[\tilde{u}_h - u_h]ds + \int_{\Gamma_0}[\beta u_h]\{\tilde{u}_h - u_h\}ds\}, \tag{4.9b}$$

$$I_3 = -\int_\Gamma \{\hat{q}_h\}\cdot[u_h]ds - \int_{\Gamma_0}[\hat{q}_h]\{u_h\}ds, \tag{4.9c}$$

$$I_4 = -\int_\Gamma \{q_h\}\cdot[\hat{u}_h - u_h]ds - \int_{\Gamma_0}[q_h]\{\hat{u}_h - u_h\}ds, \tag{4.9d}$$

Eq. (4.8) can be written as

$$\|q_h\|_2^2 + I_1 + I_2 + I_3 + I_4 = \frac{1}{\varepsilon}\int_\Omega f u_h dx. \tag{4.10}$$

As the numerical fluxes are consistent, we have $[\hat{q}_h] = 0$ and $[\hat{u}_h] = 0$ on Γ_0. As a result,

$$\begin{aligned} I_3 + I_4 &= -\int_{\Gamma\setminus\Gamma_0}\{\hat{q}_h\}\cdot[u_h]ds - \int_{\Gamma_0}\{\hat{q}_h\}\cdot[u_h]ds - \int_{\Gamma\setminus\Gamma_0}\{q_h\}\cdot[\hat{u}_h - u_h]ds \\ &\quad + \int_{\Gamma_0}\{q_h\}\cdot[u_h]ds - \int_{\Gamma_0}[q_h]\{\hat{u}_h - u_h\}ds \\ &= -\int_{\Gamma\setminus\Gamma_0}\{\hat{q}_h\}\cdot[u_h]ds - \int_{\Gamma\setminus\Gamma_0}\{q_h\}\cdot[\hat{u}_h - u_h]ds \\ &\quad - \int_{\Gamma_0}(\hat{q}_h - \{q_h\})\cdot[u_h]ds - \int_{\Gamma_0}[q_h](\hat{u}_h - \{u_h\})ds. \end{aligned} \tag{4.11}$$

Inserting the numerical fluxes defined in (3.13) and (3.14) in (4.11), we obtain

$$\begin{aligned} I_3 + I_4 &= -\int_{\Gamma\setminus\Gamma_0}\{\hat{q}_h\}\cdot[u_h]ds - \int_{\Gamma\setminus\Gamma_0}\{q_h\}\cdot[\hat{u}_h - u_h]ds + \int_{\Gamma_0} C_{11}[u_h]^T[u_h]ds \\ &= -\int_{\Gamma\setminus\Gamma_0}(\hat{q_h} - \{q_h\})\cdot[u_h]ds + \int_{\Gamma_0} C_{11}[u_h]^T[u_h]ds \\ &= \int_{\Gamma\setminus\Gamma_0} C_{11}(u_h^+)^2 ds + \int_{\Gamma_0} C_{11}[u_h]^T[u_h]ds. \end{aligned} \tag{4.12}$$

Integrating by parts and then implementing (4.1) in (4.9a) leads to

$$\begin{aligned} I_1 &= \frac{1}{\varepsilon}\int_\Omega (\beta u_h)\cdot\bigtriangledown u_h dx \\ &= -\frac{1}{\varepsilon}\int_\Omega \bigtriangledown\cdot(\beta u_h)u_h dx + \frac{1}{\varepsilon}\int_\Gamma \{\beta u_h\}\cdot[u_h]ds + \frac{1}{\varepsilon}\int_{\Gamma_0}[\beta u_h]\{u_h\}ds. \end{aligned} \tag{4.13}$$

Direct computation shows that

$$\int_{\Omega}(\beta u_h)\cdot\bigtriangledown u_h dx=\int_{\Omega}\bigtriangledown\cdot(\beta u_h)u_h dx. \tag{4.14}$$

The combination of (4.13) and (4.14) yields

$$I_1=\frac{1}{2\varepsilon}\bigg(\int_{\Gamma}\{\beta u_h\}\cdot[u_h]ds+\int_{\Gamma_0}[\beta u_h]\{u_h\}ds\bigg). \tag{4.15}$$

By (4.9b) and (4.15), we obtain

$$\begin{aligned}I_1+I_2=&\frac{1}{\varepsilon}\bigg(\frac{1}{2}\int_{\Gamma}\{\beta u_h\}\cdot[u_h]ds+\frac{1}{2}\int_{\Gamma_0}[\beta u_h]\{u_h\}ds\bigg)+\frac{1}{\varepsilon}\int_{\Gamma\backslash\Gamma_0}\{\beta u_h\}\cdot[\tilde{u}_h-u_h]ds\\&+\frac{1}{\varepsilon}\int_{\Gamma_0}\{\beta u_h\}\cdot[\tilde{u}_h-u_h]ds+\frac{1}{\varepsilon}\int_{\Gamma_0}[\beta u_h]\{\tilde{u}_h-u_h\}ds.\end{aligned} \tag{4.16}$$

Since a straightforward computation leads to

$$\int_{\Gamma_0}\{\beta u_h\}\cdot[u_h]ds=\int_{\Gamma_0}[\beta u_h]\{u_h\}ds, \tag{4.17}$$

Eqs. (4.16) and (4.17), together with the definition of $\tilde{u}_h$, yield

$$\begin{aligned}I_1+I_2=&\frac{1}{\varepsilon}\bigg(\frac{1}{2}\int_{\Gamma\backslash\Gamma_0}\{\beta u_h\}\cdot[u_h]ds+\int_{\Gamma\backslash\Gamma_0}\{\beta u_h\}[\tilde{u}_h-u_h]ds+\int_{\Gamma_0}[\beta u_h]D_{11}\cdot[u_h]ds\bigg)\\=&\frac{1}{\varepsilon}\bigg(\frac{1}{2}\int_{\Gamma\backslash\Gamma_0}(\beta\cdot\eta^{+}{u_h^{+}}^2)ds+\int_{\Gamma\backslash\Gamma_0}\{\beta u_h\}[\tilde{u}_h-u_h]ds+\int_{\Gamma_0}[u_h]^TM[u_h]ds\bigg)\\=&\frac{1}{\varepsilon}\bigg(\frac{1}{2}\int_{\Gamma^-}\beta\cdot n^{+}{u_h^{+}}^2ds+\frac{1}{2}\int_{\Gamma^+}\beta\cdot n^{+}{u_h^{+}}^2ds+\int_{\Gamma_0}[u_h]^TM[u_h]ds\\&+\int_{\Gamma^-}\{\beta u_h\}[\tilde{u}_h-u_h]ds+\int_{\Gamma^+}\{\beta u_h\}[\tilde{u}_h-u_h]ds\bigg)\\=&\frac{1}{2\varepsilon}\bigg(\int_{\Gamma^-}(-\beta\cdot n^{+}){u_h^{+}}^2ds+\int_{\Gamma^+}\beta\cdot n^{+}{u_h^{+}}^2ds+2\int_{\Gamma_0}[u_h]^TM[u_h]ds\bigg),\end{aligned} \tag{4.18}$$

where $M=diag(\beta_1D_{11}(1),\beta_2D_{11}(2))$ is a 2×2 symmetric positive definite matrix under the assumption of this theorem.

Suppose $f=0$ on the right side of (4.10). From (4.10), (4.12) and (4.18), we conclude that

$$q_h\equiv0,\ [u_h]=0,\ \text{on }\Gamma_0,\ \text{and }\ u_h=0,\text{ on }\partial\Omega. \tag{4.19}$$

Inserting (4.19) into (4.3) and implementing the consistency of the numerical fluxes in it, we have

$$\int_k\nabla u_h\cdot r dx=0,\quad\forall r\in S(k)^2,$$

which implies $\nabla u_h\ \equiv0\ on\ k$. As a result, u_h is a piecewise constant. Since $[u_h]=0$ on Γ_0 and $u_h=0$ on $\partial\Omega$, we conclude that $u_h\equiv0$. This completes the proof. □

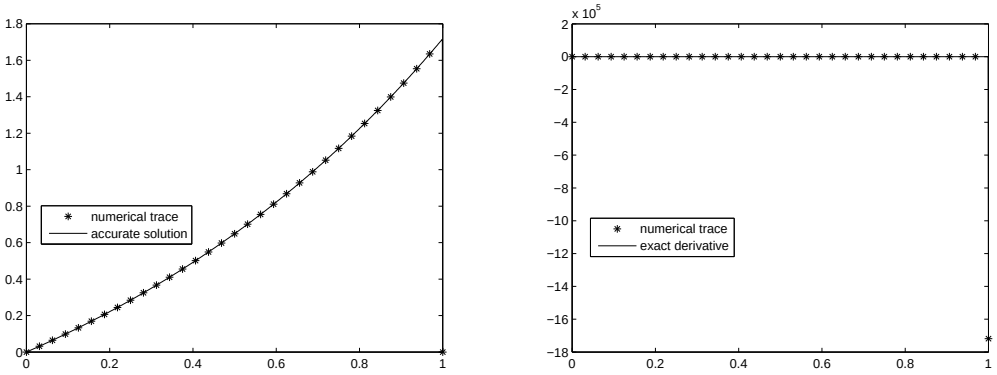

Fig. 5.1. u and $\hat{u}_h$ (left) and q and $\hat{q}_h$ (right) under uniform mesh, $N = 32$, $p = 1$, $\varepsilon = 10^{-6}$.

5. Numerical Results

5.1. One-dimensional model

In this section we present some numerical results for problem (3.1). For this purpose, we choose, in (3.1), $b = 1$ and the right-hand function $f = e^x$ with the Dirichlet boundary conditions $u_0 = u_1 = 0$. Therefore, the exact solution is given by

$$u(x) = \begin{cases} \dfrac{e^x(1-e^{-\frac{1}{\varepsilon}}) + e^{1-\frac{1}{\varepsilon}} - 1 + (1-e)e^{\frac{x-1}{\varepsilon}}}{(1-\varepsilon)(1-e^{-\frac{1}{\varepsilon}})}, & \varepsilon \neq 1, \\ \dfrac{e}{e-1}(e^x - 1) - xe^x, & \varepsilon = 1, \end{cases} \tag{5.1}$$

which exhibits a boundary layer with the width $\mathcal{O}(\varepsilon|\ln\epsilon|)$, at the outflow boundary $x = 1$. In view of this fact, we take the approximate width of the boundary layer as $\tau = (2p+1)\epsilon\ln(N+1)$.

Plotted in Fig. 5.1 are the numerical traces $\hat{u}_h$ and $\hat{q}_h$ under uniform mesh with $\varepsilon = 10^{-6}$ and $N = 32$, respectively. We see that the LDG numerical solutions do not have any oscillatory behavior even for small ε under uniform meshes. In other words, the LDG method is more local than the traditional finite element and finite difference methods.

Table 5.1: The discrete L_∞ error, under uniform mesh, $\varepsilon = 0.5$, 1-D.

	$p=1$		$p=2$		$p=3$	
i	$\|u-\hat{u}_h\|_{L_\infty}$	order	$\|u-\hat{u}_h\|_{L_\infty}$	order	$\|u-\hat{u}_h\|_{L_\infty}$	order
3	1.33e-04	2.86	9.14e-08	4.88	3.05e-11	6.89
4	1.72e-05	2.95	2.92e-09	4.97	2.44e-13	6.97
5	2.19e-06	2.97	9.26e-11	4.98	1.64e-14	—
6	2.76e-07	2.99	3.09e-12	4.91	6.63e-14	—
7	3.47e-08	2.99	9.28e-13	—	1.67e-13	—
i	$\|q-\hat{q}_h\|_{L_\infty}$	order	$\|q-\hat{q}_h\|_{L_\infty}$	order	$\|q-\hat{q}_h\|_{L_\infty}$	order
3	6.22e-04	2.90	4.59e-07	4.92	1.58e-10	6.94
4	8.04e-05	2.95	1.46e-08	4.97	1.26e-12	6.96
5	1.02e-05	2.97	4.63e-10	4.98	9.91e-14	—
6	1.29e-06	2.99	1.44e-11	5.00	4.00e-13	—
7	1.62e-07	2.99	3.78e-12	—	7.99e-13	—

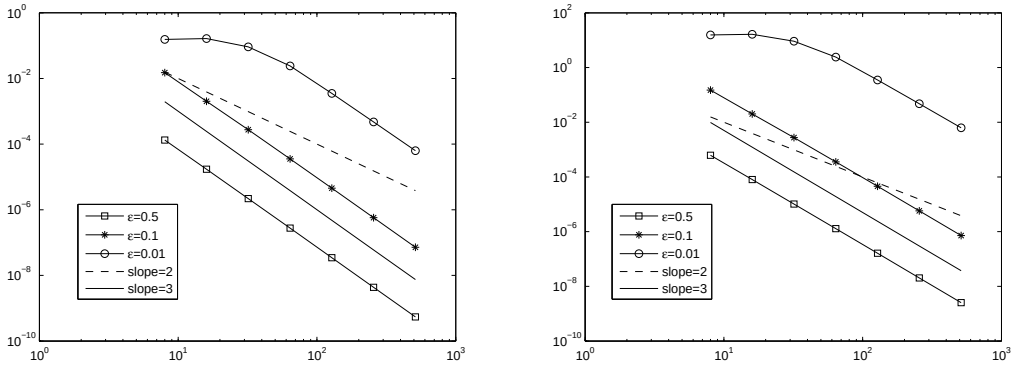

Fig. 5.2. Convergence curve of $\hat{u}_h$ (left) and $\hat{q}_h$ (right) under uniform mesh for 1-D, $p = 1$.

Throughout this section, the errors in the discrete L_∞ norm at nodes $x_{j+\frac{1}{2}}$ are denoted by

$$\|u - \hat{u}_h\|_{L_\infty} = \max_{0\le j\le N} \left|u(x_{j+\frac{1}{2}}) - \hat{u}_h(x_{j+\frac{1}{2}})\right|,$$
$$\|q - \hat{q}_h\|_{L_\infty} = \max_{0\le j\le N} \left|q(x_{j+\frac{1}{2}}) - \hat{q}_h(x_{j+\frac{1}{2}})\right|.$$

In the legend of figures, S-mesh and G-mesh demonstrate the Shishkin mesh and improved grade mesh, respectively. Listed in Tables 5.1-5.2 are the errors and numerically observed convergence order with polynomial orders varying from $p = 1$ to $p = 3$ for a discrete L_∞ norm for $\epsilon = 0.5$ and $\varepsilon = 0.05$, respectively. The first row shows the degree p of the polynomials we use to approximate the unknowns u and q. The first column is the mesh number, where $i = 3, 4, \cdots, 7$ indicates a mesh with $N = 2^i$ elements. As shown in Tables 5.1-5.2, the convergence rate for the discrete L_∞ norm of $\hat{u}_h$ and $\hat{q}_h$ at the nodes $x_{j+\frac{1}{2}}$ is $2p + 1$. Plotted in Fig. 5.2 are the corresponding convergence curves of the numerical traces for $\varepsilon = 0.5$, $\varepsilon = 0.1$ and $\varepsilon = 0.01$, respectively, when $p = 1$. Though the $2p+1$ superconvergence rate is observed, the error bound is strongly dependent on ε.

In the following, we turn to the LDG method based on the Shishkin and improved grade meshes. Listed in Tables 5.3-5.4 are the errors in the discrete L_∞ norm of the numerical traces and the corresponding convergence rates with $\varepsilon = 10^{-4}$ and $\varepsilon = 10^{-6}$ for Shishkin and improved

Table 5.2: The discrete L_∞ error under uniform mesh, $\varepsilon = 0.05$, 1-D.

	$p = 1$		$p = 2$		$p = 3$	
i	$\|u - \hat{u}_h\|_{L_\infty}$	order	$\|u - \hat{u}_h\|_{L_\infty}$	order	$\|u - \hat{u}_h\|_{L_\infty}$	order
3	6.71e-02	1.20	4.38e-03	2.95	1.44e-04	4.81
4	1.43e-02	2.23	2.38e-04	4.20	1.97e-06	6.19
5	1.92e-03	2.90	7.85e-06	4.92	1.60e-08	6.94
6	2.61e-04	2.88	2.62e-07	4.91	1.32e-10	6.92
7	3.38e-05	2.95	8.37e-09	4.97	9.09e-13	7.18
i	$\|q - \hat{q}_h\|_{L_\infty}$	order	$\|q - \hat{q}_h\|_{L_\infty}$	order	$\|q - \hat{q}_h\|_{L_\infty}$	order
3	1.34e-00	1.20	8.76e-02	2.95	2.88e-03	4.81
4	2.86e-01	2.23	4.77e-03	4.20	3.93e-05	6.19
5	3.83e-02	2.90	1.57e-04	4.92	3.20e-07	6.94
6	5.22e-03	2.88	5.23e-06	4.91	2.64e-09	6.92
7	6.76e-04	2.95	1.67e-07	4.97	3.58e-11	6.21

Table 5.3: The numerical results on Shishkin mesh for 1-D.

		$\varepsilon = 10^{-4}$				$\varepsilon = 10^{-6}$			
p	i	$\|\hat{e}_u\|_{L_\infty}$	order	$\|\hat{e}_q\|_{L_\infty}$	order	$\|\hat{e}_u\|_{L_\infty}$	order	$\|\hat{e}_q\|_{L_\infty}$	order
1	4	8.67e-03	1.65	5.05e-03	1.65	8.67e-03	1.65	5.05e-03	1.65
	5	2.06e-03	2.07	1.20e-03	2.07	2.06e-03	2.07	1.20e-03	2.07
	6	4.73e-04	2.12	2.75e-04	2.12	4.73e-04	2.12	2.75e-04	2.12
	7	9.77e-05	2.28	5.68e-05	2.28	9.77e-05	2.28	5.68e-05	2.28
	8	1.87e-05	2.39	1.09e-05	2.39	1.87e-05	2.39	1.09e-05	2.39
2	4	1.07e-03	2.44	6.23e-04	2.44	1.07e-03	2.44	6.22e-04	2.44
	5	1.19e-04	3.16	6.95e-05	3.16	1.19e-04	3.16	6.95e-05	3.16
	6	9.09e-06	3.71	5.29e-06	3.71	9.09e-06	3.71	5.29e-06	3.71
	7	6.48e-07	3.81	3.77e-07	3.81	6.48e-07	3.81	3.77e-07	3.81
	8	4.04e-08	4.00	2.35e-08	4.00	4.09e-08	3.99	2.38e-08	3.99
3	4	1.30e-04	3.25	7.59e-05	3.25	1.30e-04	3.25	7.59e-05	3.25
	5	7.04e-06	4.21	4.10e-06	4.21	7.04e-06	4.21	4.10e-06	4.21
	6	2.16e-07	5.02	1.26e-07	5.02	2.16e-07	5.03	1.26e-07	5.03
	7	5.07e-09	5.42	2.95e-09	5.42	5.87e-09	5.20	3.42e-09	5.20
	8	8.84e-11	5.84	5.07e-11	5.86	3.82e-10	–	2.22e-10	–

Table 5.4: The numerical results on improved grade mesh for 1-D.

		$\varepsilon = 10^{-4}$				$\varepsilon = 10^{-6}$			
p	i	$\|\hat{e}_u\|_{L_\infty}$	order	$\|\hat{e}_q\|_{L_\infty}$	order	$\|\hat{e}_u\|_{L_\infty}$	order	$\|\hat{e}_q\|_{L_\infty}$	order
1	4	5.40e-03	1.79	3.14e-03	1.79	5.40e-03	1.79	3.14e-03	1.79
	5	9.68e-04	2.48	5.63e-04	2.48	9.68e-04	2.48	5.63e-04	2.48
	6	1.51e-04	2.68	8.82e-05	2.68	1.51e-04	2.68	8.82e-05	2.68
	7	2.25e-05	2.75	1.31e-05	2.75	2.25e-05	2.75	1.31e-05	2.75
	8	3.20e-06	2.81	1.86e-06	2.81	3.19e-06	2.81	1.86e-06	2.81
2	4	3.74e-04	3.05	2.18e-04	3.05	3.74e-04	3.05	2.18e-04	3.05
	5	1.85e-05	4.34	1.08e-05	4.34	1.85e-05	4.34	1.08e-05	4.34
	6	8.54e-07	4.44	4.97e-07	4.44	8.54e-07	4.44	4.97e-07	4.44
	7	3.41e-08	4.65	1.99e-08	4.65	3.41e-08	4.65	1.99e-08	4.65
	8	1.31e-09	4.71	7.60e-10	4.71	1.31e-09	4.71	7.60e-10	4.71
3	4	2.69e-05	4.24	1.57e-05	4.24	2.69e-05	4.24	1.57e-05	4.24
	5	4.08e-07	6.04	2.37e-07	6.04	4.08e-07	6.04	2.37e-07	6.04
	6	5.35e-09	6.25	3.11e-09	6.25	5.35e-09	6.25	3.11e-09	6.25
	7	5.89e-11	6.50	3.43e-11	6.50	5.89e-11	6.50	3.43e-11	6.50
	8	4.90e-13	6.91	3.51e-13	6.61	5.68e-13	6.70	3.49e-13	6.62

grade meshes, separately. The corresponding convergence curves are plotted in Figs. 5.3-5.4. As the derivative u' becomes very large in the boundary layer when ε is small, instead of the absolute error, the error in terms of q_h in Tables 5.3-5.4 and Figs. 5.3 (right) and Fig. 5.4 (right) is the relative one, i.e., $\|u' - q_h\|_\infty / \|u'\|_\infty$.

The $2p+1$ order uniform superconvergence of the LDG solution is clearly observed numerically, as the bound of errors is independent of ϵ. The numerical results in Tables 5.3-5.4 and Figs. 5.3-5.4 also show that the improved grade mesh works better than Shishkin mesh. Numerically it seems that the error estimates of the LDG solutions under both meshes with $\tau = (2p+1)\epsilon \log(N+1)$ are

$$\|\hat{e}_u\|_\infty < C\Big(\frac{\ln N}{N}\Big)^{2p+1}, \quad \|\hat{e}_q\|_\infty < C\Big(\frac{\ln N}{N}\Big)^{2p+1} |u|_{1,\infty}.$$

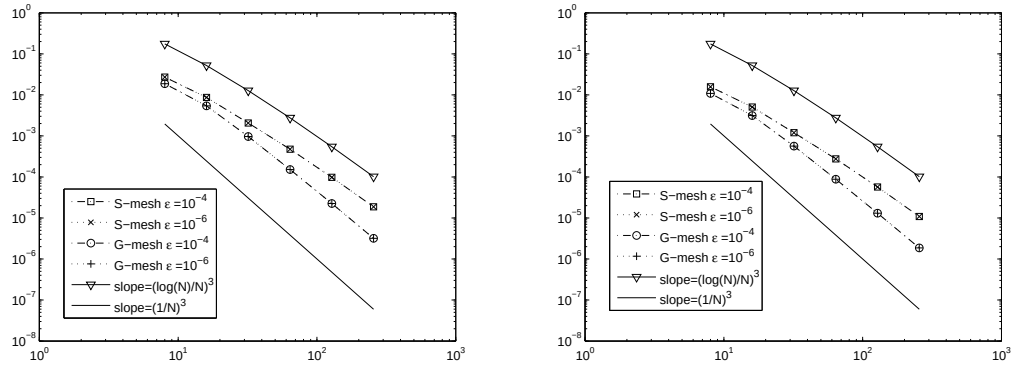

Fig. 5.3. Convergence curve of $\hat{u}_h$ (left) and $\hat{q}_h$ (right) for 1-D, $p = 1$, with layer adapted meshes.

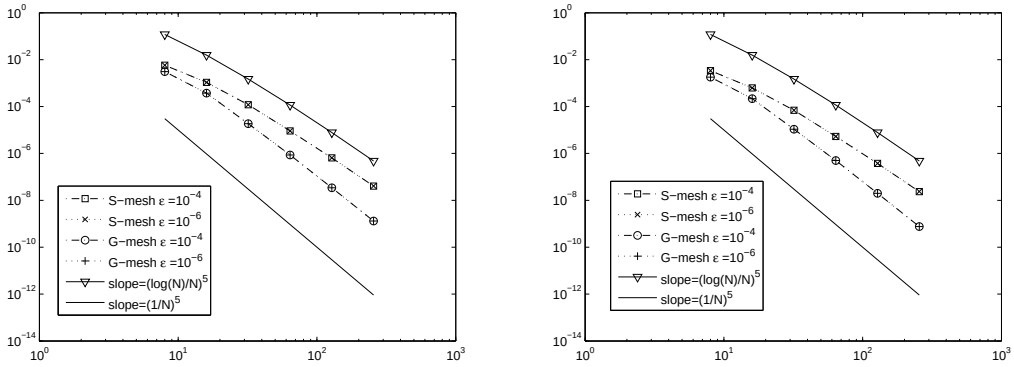

Fig. 5.4. Convergence curve of $\hat{u}_h$ (left) and $\hat{q}_h$ (right) for 1-D, $p = 2$, with layer adapted meshes.

It is worthwhile to point out that the constants C are completely independent of the singular perturbation parameter ϵ.

5.2. Two-dimensional model

This section is to demonstrate the numerical results of the LDG methods for solving (3.8). For this purpose, we choose $\vec{\beta}(x, y) = (1, 1)$ and

$$f(x,y) = (x+y)\Big(1 - e^{-\frac{1-x}{\varepsilon}} \cdot e^{-\frac{1-y}{\varepsilon}}\Big) + (x-y)\Big(e^{-\frac{1-y}{\varepsilon}} - e^{-\frac{1-x}{\varepsilon}}\Big),$$

in (3.8). Actually the corresponding exact solution is $u(x, y) = xy(1 - e^{-\frac{1-x}{\varepsilon}})(1 - e^{-\frac{1-y}{\varepsilon}})$. Clearly the boundary layer is located at the neighborhood of $x = 1$ and $y = 1$.

According to the theory of the singularly perturbed problems in terms of (3.8), the width of the boundary layer is also of order $\mathcal{O}(\epsilon|\ln\epsilon|)$. To simulate the width of the boundary layer, we take $\tau = \tau_x = \tau_y = (2p+1)\epsilon\ln(N+1)$ when the layer-adapted mesh is used. Tables 5.5-5.6 illustrate the discrete L_∞ norm at nodes for $\hat{u}_h$ under uniform mesh with $\varepsilon = 0.1$ and $\varepsilon = 0.05$, respectively. Plotted in Fig. 5.5 are the corresponding convergence curves under uniform mesh with $\varepsilon = 0.5$, $\varepsilon = 0.1$ and $\varepsilon = 0.01$ for $p = 1$ and $p = 2$, respectively. From Tables 5.5-5.6 and Fig. 5.5, the superconvergence rate $2p+1$ is clearly observed. However the error is also strongly dependent on ϵ. To overcome this difficulty, we turn to the LDG method based on the Shishkin and improved grade meshes.

Table 5.5: The discrete L_∞ error under uniform mesh, $\varepsilon = 0.1$, 2-D.

	$p=1$		$p=2$		$p=3$	
i	$\|u-\hat{u}_h\|_{L_\infty}$	order	$\|u-\hat{u}_h\|_{L_\infty}$	order	$\|u-\hat{u}_h\|_{L_\infty}$	order
3	1.33e-02	2.23	2.71e-04	4.14	2.90e-06	6.06
4	1.65e-03	3.01	8.35e-06	5.02	2.37e-08	6.93
5	2.12e-04	2.96	2.64e-07	4.98	2.18e-10	—
6	2.71e-05	2.97	8.35e-09	4.98	2.86e-12	—
7	3.43e-06	2.98	2.63e-10	4.99	—	—

Table 5.6: The discrete L_∞ error under uniform mesh, $\varepsilon = 0.05$, 2-D.

	$p=1$		$p=2$		$p=3$	
i	$\|u-\hat{u}_h\|_{L_\infty}$	order	$\|u-\hat{u}_h\|_{L_\infty}$	order	$\|u-\hat{u}_h\|_{L_\infty}$	order
3	6.65e-02	1.05	4.67e-03	2.72	1.70e-04	4.58
4	1.23e-02	2.43	2.28e-04	4.35	2.18e-06	6.29
5	1.59e-03	2.95	7.26e-06	4.97	1.69e-08	7.01
6	2.09e-04	2.93	2.33e-07	4.96	1.33e-10	6.98
7	2.70e-05	2.95	7.44e-09	4.97	—	—

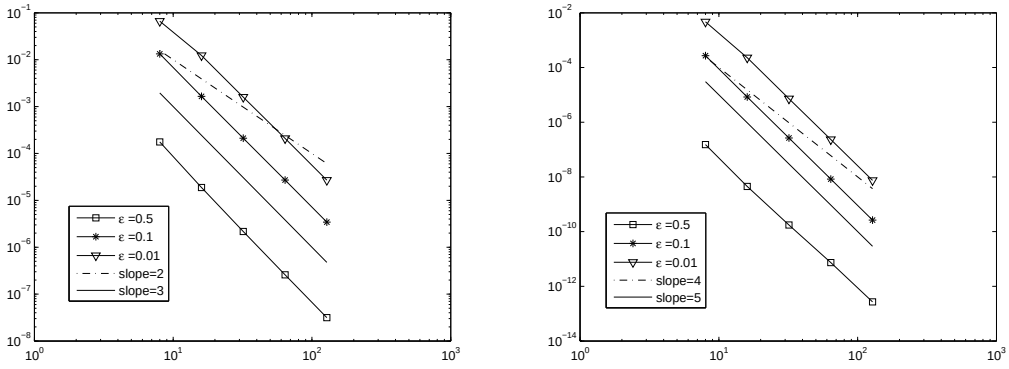

Fig. 5.5. Convergence curve of $\hat{u}_h$ for $p=1$ (left) and $p=2$ (right) under uniform mesh for 2-D, $p=1$.

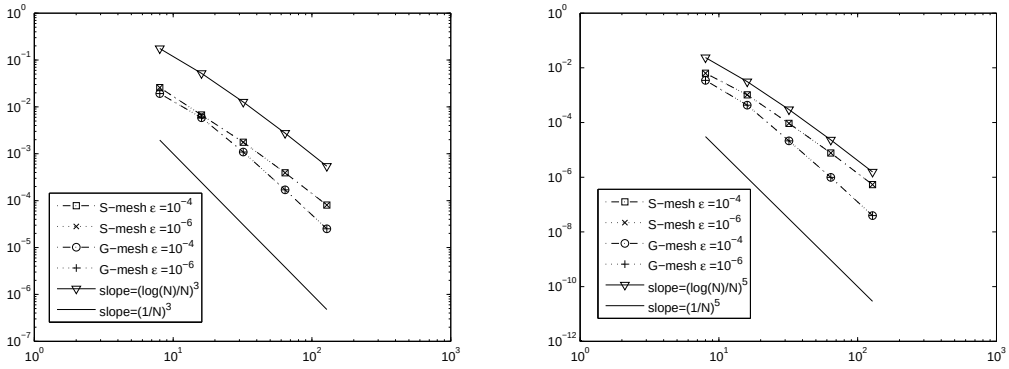

Fig. 5.6. Convergence curve of $\hat{u}_h$ for $p=1$ (left) and $p=2$ (right) for 2-D, with layer adapted mesh.

Listed in Tables 5.7-5.8 are the errors in the discrete L_∞ norm for u_h and the corresponding convergence rates with $\varepsilon = 10^{-2}$, $\varepsilon = 10^{-4}$ and $\varepsilon = 10^{-6}$ for the Shishkin and improved grade meshes, respectively. The corresponding convergence rates are plotted in Fig. 5.6. From Tables

Table 5.7: The numerical results for 2-D under Shishkin mesh.

		$\varepsilon = 10^{-2}$		$\varepsilon = 10^{-4}$		$\varepsilon = 10^{-6}$	
p	i	$\|u - \hat{u}_h\|_{L_\infty}$	order	$\|u - \hat{u}_h\|_{L_\infty}$	order	$\|u - \hat{u}_h\|_{L_\infty}$	order
1	3	2.60e-02	1.31	2.58e-02	1.33	2.58e-02	1.33
	4	6.79e-03	1.94	6.73e-03	1.94	6.73e-03	1.94
	5	1.77e-03	1.94	1.76e-03	1.94	1.76e-03	1.94
	6	3.94e-04	2.17	3.93e-04	2.16	3.93e-04	2.16
	7	8.12e-05	2.28	8.06e-05	2.29	8.05e-05	2.29
2	3	6.37e-03	1.73	6.32e-03	1.76	6.32e-03	1.76
	4	1.06e-03	2.58	1.03e-03	2.61	1.03e-03	2.61
	5	9.67e-05	3.46	9.26e-05	3.48	9.26e-05	3.48
	6	7.97e-06	3.60	7.71e-06	3.59	7.71e-06	3.59
	7	5.51e-07	3.85	5.37e-07	3.84	5.37e-07	3.84
3	3	1.43e-03	2.26	1.42e-03	2.30	1.42e-03	2.30
	4	1.44e-04	3.31	1.39e-04	3.35	1.39e-04	3.35
	5	6.82e-06	4.40	6.42e-06	4.44	6.42e-06	4.44
	6	1.77e-07	5.27	1.70e-07	5.24	1.69e-07	5.24

Table 5.8: The numerical results for 2-D under improved grade mesh.

		$\varepsilon = 10^{-2}$		$\varepsilon = 10^{-4}$		$\varepsilon = 10^{-6}$	
p	i	$\|u - \hat{u}_h\|_{L_\infty}$	order	$\|u - \hat{u}_h\|_{L_\infty}$	order	$\|u - \hat{u}_h\|_{L_\infty}$	order
1	3	1.92e-02	2.58	1.92e-02	2.65	1.92e-02	2.65
	4	5.77e-03	1.73	5.86e-03	1.71	5.86e-03	1.71
	5	1.05e-03	2.45	1.09e-03	2.43	1.09e-03	2.43
	6	1.65e-03	2.67	1.70e-04	2.67	1.70e-04	2.67
	7	2.45e-05	2.76	2.51e-05	2.76	2.51e-05	2.76
2	3	3.45e-03	3.62	3.48e-03	3.72	3.48e-03	3.72
	4	4.17e-04	3.05	4.30e-04	3.02	4.30e-04	3.02
	5	2.03e-05	4.36	2.14e-05	4.33	2.14e-05	4.33
	6	9.50e-07	4.42	9.85e-07	4.44	9.85e-07	4.44
	7	3.80e-08	4.64	3.94e-08	4.64	3.94e-08	4.64
3	3	5.81e-04	4.89	5.89e-04	5.03	5.89e-04	5.04
	4	2.99e-05	4.28	3.13e-05	4.24	3.13e-05	4.24
	5	4.58e-07	6.03	4.72e-07	6.05	4.73e-07	6.05
	6	5.89e-09	6.28	6.21e-09	6.25	6.21e-09	6.25

5.7-5.8 and Fig. 5.6, we see that the error bound is independent of ε. This fact seems to indicate that

$$\|\hat{e}_u\|_\infty < C\Big(\frac{\ln N}{N}\Big)^{2p+1}.$$

Once again C is independent of ε.

Remark 5.1. When taking $\tau = (2p+1)\epsilon|\ln\epsilon|$, we also obtained the corresponding numerical results under both the Shishkin and improved grade meshes. The unform superconvergence rate $\mathcal{O}(N^{-(2p+1)})$ is also obtained for these two layer adapted meshes. For simplicity, we only list the corresponding results for 2-D case based on the improved graded mesh in Table 5.9.

Remark 5.2. 2-D problems require smaller h to get into the asymptotic range. We believe that the data in Tables 5.7 and 5.8 are still in pre-asymptotic phase.

Table 5.9: The numerical results for 2-D under improved grade mesh, $\tau = (2p+1)\varepsilon|\ln\varepsilon|$.

		$\varepsilon = 10^{-2}$		$\varepsilon = 10^{-4}$		$\varepsilon = 10^{-6}$	
p	i	$\|u-\hat{u}_h\|_{L_\infty}$	order	$\|u-\hat{u}_h\|_{L_\infty}$	order	$\|u-\hat{u}_h\|_{L_\infty}$	order
1	3	4.95e-02	0.35	3.22e-02	0.14	5.64e-02	0.40
	4	7.56e-03	2.71	1.33e-02	1.27	1.55e-02	1.86
	5	1.27e-03	2.57	2.02e-03	2.72	2.58e-03	2.59
	6	1.77e-04	2.85	3.00e-04	2.75	4.02e-04	2.68
	7	2.35e-05	2.91	4.01e-05	2.90	5.41e-05	2.89
2	3	1.13e-02	0.94	6.72e-03	0.15	1.67e-02	0.63
	4	5.47e-04	4.36	1.36e-03	2.31	2.18e-03	2.94
	5	2.96e-05	4.21	7.05e-05	4.27	1.10e-04	4.31
	6	1.05e-06	4.81	2.57e-06	4.78	4.12e-06	4.74
	7	3.57e-08	4.88	8.68e-08	4.89	1.43e-07	4.85
3	3	2.65e-03	1.59	1.23e-03	0.52	4.88e-03	0.87
	4	4.68e-05	5.82	1.38e-04	3.15	2.95e-04	4.05
	5	7.11e-07	6.04	2.50e-06	5.79	4.75e-06	5.96
	6	7.05e-09	6.66	2.41e-08	6.70	4.79e-08	6.63

6. Conclusion

In this paper, the LDG method was implemented to solve the singularly perturbed convection-diffusion equations. The existence and uniqueness of the LDG solution is verified first. Then, under the uniform and two-type layer-adapted meshes in one and two dimensional settings, numerically we demonstrate that the combination of DG methods and the layer-adapted meshes is a robust approach for solving singularly perturbed problems. Our numerical results show that the LDG method does not produce any oscillation even under the uniform mesh for 1-D and 2-D models. More significantly, under Shishkin and improved grade meshes, the $2p+1$-order uniform superconvergence of numerical fluxes are observed for both 1-D and 2-D cases. This uniform superconvergence result, especially for 2-D case, is a remarkable observation which is reported for the first time in the literature to our knowledge. The theoretical verification of uniform convergence and superconvergence in the one dimensional setting is our on-going work.

Acknowledgments. Supported by the National Natural Science Foundation of China (10571053, 10871066) and the Programme for New Century Excellent Talents in University (NCET-06-0712).

References

[1] D.N. Arnold, F. Brezzi, B. Cockburn and L.D. Marini, Unified analysis of discontinuous Galerkin methods for elliptic problems, *SIAM J. Numer. Anal.*, **39** (2002), 1749-1779.

[2] F. Bassi and S. Rebay, A high-order accurate discontinuous finite element method for the numerical solution of the compressible Navier-Stokes equations, *J. Comput. Phys.*, **131** (1997), 267-279.

[3] C.E. Baumann and J.T. Oden, A discontinuous *hp* finite element method for convection-diffusion problems, *Comput. Method. Appl. Mech. Eng.*, **175** (1999), 311-341.

[4] K.S. Bey and J.T. Oden, *hp*-version discontinuous Galerkin method for hyperbolic conservation laws, *Comput. Method. Appl. Mech. Eng.*, **133** (1996), 259-286.

[5] K.S. Bey, J.T. Oden, and A. Patra, *hp*-version discontinuous Galerkin method for hyperbolic conservation laws: A parallel strategy, *Int. J. Numer. meth. Eng.*, **38** (1995), 3889-3908.

[6] W. Castaings and I.M. Navon, Mesh refinement strategies for solving singularly perturbed reaction-diffusion problems, *Comput. Math. Appl.*, **41** (2001), 157-176.

[7] P. Castillo, B. Cockburn, D. Schtzau, and C. Schwab, Optimal a priori error estimates for the *hp*-version of the LDG method for convection diffusion problems, *Math. Comput.*, **71(238)** (2002), 455-478.

[8] P. Castillo, An optimal error estimate for the local discontinuous Galerkin method, Proceedings of the First International Symposium on Discontinuous Galerkin Methods (G.E. Karniadakis B. Cockburn and C.-W. Shu, eds.), Lecture Notes in Computational Science and Engineering, Springer, 2000, 285-290.

[9] P. Castillo, B. Cockburn, I. Perugia, and D. Schötzau, An a priori error analysis of the local discontinuous Galerkin method for elliptic problems, *SIAM J. Numer. Anal.*, **38** (2000), 1676-1706.

[10] F. Celiker and B. Cockburn, Superconvergence of the numerical traces of discontinuous Galerkin and hybridized methods for convection-diffusion problems in one space dimension, *Math. Comput.*, **76** (2007), 67-96.

[11] B. Cockburn and C.-W. Shu, The local discontinuous Galerkin method for time-dependent convection-diffusion systems, *SIAM. J. Numer. Anal.*, **35** (1998), 2440-2463.

[12] B. Cockburn and C.-W. Shu, TVB Runge-Kutta local projection discontinuous Galerkin methods for scalar conservation laws II: General framework, *Math. Comput.*, **52** (1989), 411-435.

[13] B. Cockburn, S.Y. Lin, and C.-W. Shu, TVB Runge-Kutta local projection discontinuous Galerkin methods for scalar conservation laws III: One dimensional systems, *J. Comput. Phys.*, **84** (1989), 90-113.

[14] B. Cockburn, S. Hou, and C.-W. Shu, TVB Runge-Kutta local projection discontinuous Galerkin methods for scalar conservation laws IV: The multidimensional case, *Math. Comput.*, **54** (1990), 545-581.

[15] B. Cockborn, G.E. Karniadakis, and C.-W. Shu, The development of discontinuous Galerkin methods, Discontinuous Galerkin Methods: Theory, Computation and Applications, (Berlin) (B. Cockborn, G. E. karniadakis and C.-W.Shu, eds.), Lecture Notes in Comput. Sci. Engrg., Vol 11, Springer-Verlag, Feb (2000), 3-50.

[16] B. Cockburn, G. Kanschat, I. Perugia, and D. Schtzau, Superconvergence of the local discontinuous Galerkin method for elliptic problems on Cartesian grids, *SIAM J. Numer. Anal.*, **39** (2001), 264-285.

[17] R.G. Duran and L. Lomhardi, Finite element approximation of convection diffusion problems using grade meshes, *Appl. Numer. Math.*, **56** (2006), 1314-1325.

[18] K. Ericksson and C. Johnson, Adaptive finite element methods for parabolic problems I: A linear model problem, *SIAM J. Numer. Anal.*, **28** (1991), 12-23.

[19] K. Ericksson and C. Johnson, Adaptive finite element methods for parabolic problems II: Optimal error estimates in $l_\infty l_2$ and $l_\infty l_\infty$, *SIAM J. Numer. Anal.*, **32** (1995), 706-740.

[20] P. Lesaint and P.A. Ravirt, On a finite element method for solving the neutron transport equation. In C. De Boor, editor, Mathematical Aspects of Finite Elements in Partial Differential Equations, pages 89-145, Academic Press, 1974.

[21] J.C. Li and Y.T. Chen, Uniform convergence analysis for singularly perturbed elliptic problems with parabolic layers, *Numer. Math. Theor. Meth. Appl.*, **1** (2008), 138-149.

[22] T. Linß and H.-G. Roos, Sufficient conditions for uniform convergence on layer-adapted grids, *Computing*, **63** (1999), 27-45.

[23] T. Linß and M. Stynes, Numerical methods on Shishkin meshes for linear convection-diffusion problems, *Comput. Meth. Appl. Mech. Eng.*, **190** (2001), 3527-3542.

[24] E. O'Riordan, J. Stynes and M. Stynes, A parameter-uniform finite difference method for a coupled system of convection-diffusion two-point boundary value problems, *Numer. Math. Theor. Meth. Appl.*, **1** (2008), 176-197.

[25] W.H. Reed and T.R. Hill, Triangular mesh methods for the neutron transport equation. Technical Report LA-UR-73-479, Los Alamos Scientific Laboratory, Los Alamos, 1973.

[26] H.-G. Roos and T. Skalicky, A comparison of the finite element method on Shishkin and Gartland-type meshes for convection diffusion problems, *CWI Quarterly*, **10** (1997), 277-300.

[27] H.-G. Roos, M. Stynes, and L. Tobiska, Numerical Methods for Singularly Perturbed Differential Equations, Springer, Berlin, 1996.

[28] A.H. Schatz and L.B. Wahlbin, On the finite element method for singularly perturbed reaction-diffusion problems in two and one dimensions, *Math. Comput.*, **40** (1983), 47-89.

[29] C. Schwab and M. Suri, The p and hp versions of the finite element method for problems with boundary layers, *Math. Comput.*, **65** (1996), 1403-1429.

[30] G.I. Shishkin, A finite difference scheme on a priori adapted meshes for a singularly perturbed parabolic convection-diffusion equation, *Numer. Math. Theor. Meth. Appl.*, **1** (2008), 214-234.

[31] L.B. Wahlbin, Local behavior in finite element methods, in Handbook of Numerical Analysis, Vol. II, P.G.Ciarlet and J.L.Lion eds., North-Holland Publishing Company, Amsterdam, (1991), 353-522.

[32] T.P. Wihler and C. Schwab, Robust exponential convergence of the hp discontinuous Galerkin FEM for convection-diffusion problems in one space dimension, *East-West J. Numer. Math.*, **8** (2000), No.1, 57-70.

[33] C. Xenophontos, The hp finite element method for singularly perturbed problems, Ph.D. Dissertation, Univ. of Maryland, Baltimore, County, 1996.

[34] Z.Q. Xie and Z. Zhang, Superconvergence of DG method for one-dimensilonal singularly perturbed problems, *J. Comput. Math.*, **25** (2007), 185-200.

[35] Z. Zhang, Superconvergent approximation of singularly perturbed problems, *Numer. Meth. PDEs*, **18** (2002), 374-395.

[36] Z. Zhang, Finite element superconvergence on Shishkin mesh for 2-D convection-diffusion problems, *Math. Comput.*, **72** (2003), 1147-1177.

[37] Z.Z. Zhang, Z.Q. Xie, and Z. Zhang, Superconvegence of discontinuous Galerkin methods for convection-diffusion problems, summited to *J. Sci. Comp.*.